Electron acceleration from the interaction of Vulcan 100TW laser with Au foils and its dependence on laser polarisation

S. R. Nagel, C. Bellei, S. Kneip, S. P. D. Mangles, C. Palmer, L. Willingale, A. E. Dangor and Z. Najmudin

Blackett Laboratory, Imperial College London, London SW7 2BZ, UK

R. J. Clarke and R. Heathcote

Central Laser Facility, STFC, Rutherford Appleton Laboratory, HSIC, Didcot, Oxon OX11 0QX, UK

Contact | s.nagel@imperial.ac.uk

B. Dromey, S. Kar, K. Markey, P. Simpson and M. Zepf

Queen's University Belfast, Belfast BT7 1NN, UK

M. Kaluza and A. Sävert

Institut für Quantenoptik, Friedrich-Schiller-Universität Jena, Germany

A. Henig and J. Schreiber

Max-Planck-Institut für Quanten Optik, Garching, Germany

Abstract

In this report electron acceleration from overdense plasmas is investigated by conducting thickness scans using Au foil targets ranging from thicknesses of 10 to 100 μm. In addition the effects of linear and circular polarisation are observed. The electron spectra, of the most energetic electrons produced in the interaction, are measured along the laser direction and extend up to 40 MeV. A decrease in number and effective temperature of energetic electrons is observed for circular polarisation as compared to linear polarisation. Simultaneously the proton beam profiles emitted normal to the target rear surface also indicate a dependence on electron beam recirculation.

Introduction

Light cannot normally propagate into overdense plasma, above the critical density, n_c, defined as the density at which $\omega=\omega_p$, where ω is the laser frequency and $\omega_p=(n_e e^2/m_e/\varepsilon_0)^{1/2}$ is the plasma frequency. However laser energy can be absorbed by electrons at the critical surface. Energy can then be transferred to ions by space charge fields set up as energetic electrons leave the target. The ions are accelerated and emitted as collimated beams from the target rear surface [1,2].

The main electron acceleration mechanisms from solid targets are resonance absorption [3], vacuum or Brunel heating [4], and J×B heating. For J×B heating the intensity of the laser light has to be high enough to make the electrons move relativistically in the fields, i.e. the electrons have $v_{osc} \approx c$. At these intensities the magnetic field component of the Lorentz force becomes comparable to the electric field component. At the vacuum plasma boundary, the electrons oscillating in the electric field will be directed into the forward direction by the magnetic field twice during a single laser oscillation. This leads to bunching of the electrons at 2ω from J×B heating [3]. Unlike resonance or vacuum heating, the J×B heating occurs most efficiently at normal incidence to the plasma.

Considering a linearly polarised wave propagating in x $\vec{E}=E_0(x)\hat{y}\sin(\omega t)$, with the ponderomotive force,

$\vec{F_p}=-\frac{q}{4\langle\gamma\rangle m_e\omega^2}\nabla\langle E^2\rangle$, then the linearly polarised wave gives rise to a longitudinal force term:

$$f_x=-\frac{\langle\gamma\rangle m_e c^2}{4}\frac{\partial\langle a_0^2\rangle}{\partial x}(1-\cos(2\omega t))$$

where a_0 is the normalised vector potential. The first term on the RHS is the usual DC ponderomotive force, which in this context tends to push the electron density profile inwards (hole boring). The high frequency component leads to heating for any polarisation apart from circular, for which it disappears.

Experimental setup

The experiment described, was performed using the Vulcan laser. Figure 1 shows a sketch of the experimental setup. For this experiment the OPCPA front end was used to reduce the pulse length in TAW. Therefore the laser had a duration of (642±124) fs indicating a pulse length of $c\tau$ = (193±37) μm and an energy of (55±4) J on target. The operation wavelength of Vulcan is 1054 nm. For this wavelength the non-relativistic critical electron density is n_c =1×10^{21} cm^{-3}. An *f*/3 off-axis parabolic mirror focuses the laser onto the solid targets. The targets were gold foils with thicknesses between 10 and 100 μm. Spot size measurements give a FWHM of 9.5 μm, this implies intensities between 4.8×10^{19} Wcm^{-2} and 8.1×10^{19} Wcm^{-2}. Therefore the normalized vector potential, a_0, lies between 5.9 and 7.8.

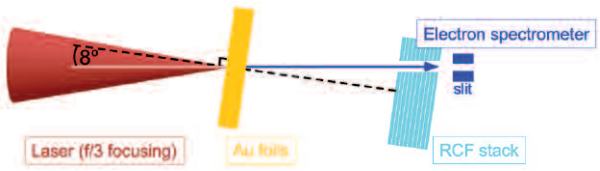

Figure 1. Schematic of the experimental setup.

The laser polarisation can be changed from linear to circular, by putting a $\lambda/4$ wave plate in the collimated beam. The angle of incidence is 8° off target normal, the electron spectra are measured along the laser axis using a magnetic spectrometer. The proton data is taken simultaneously using RCF stacks, situated 7 cm behind focus, and placed parallel to the target. These stacks have slits in them in order to allow the electrons to propagate undisturbed. Image plate is used as the electron detector.

Experimental results

The electron spectra taken are shown in Figure 2, (a) linear laser polarisation and (b) circular laser polarisation. The different colours correspond to different target thicknesses. The number of electrons per MeV per steradian is plotted against the electron energy in MeV. Both laser polarisations lead to the same intensity on target. In general thicker targets show a higher number of electrons, see figure 3 (exception 50 µm linear). For circular polarisation a lower number of electrons is observed. The shot for 50 µm linear polarisation is abnormal in the case of number. The temperature of the spectra was obtained by fitting a quasi-maxwellian: $y = A^*\exp(-E/T_{eff})$.

Figure 4 shows the effective temperatures vs. the target thicknesses for the two different polarisations. The effective temperatures measured are comparable to those estimated by Wilks[5]:

$$T_{hot} = mc^2(\gamma - 1) = mc^2[\sqrt{1 + a_0^2} - 1]$$
$$= [\sqrt{1 + 0.74 I_{18}\lambda_{\mu}^2} \; 1] \times 511 keV$$

With the wavelength and the intensity in this experiment, one would expect $T_{hot} \approx 3.5$MeV.

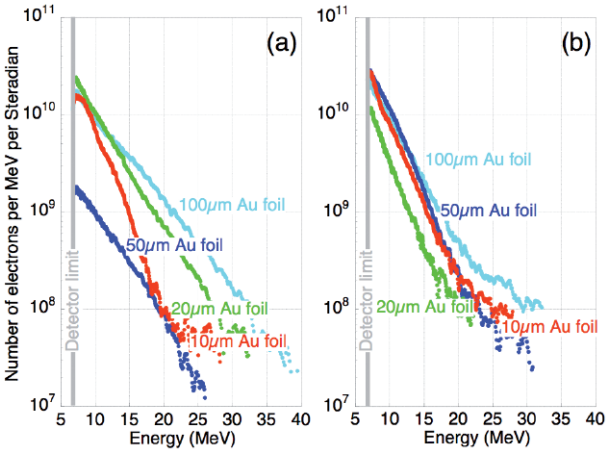

Figure 2. Electron spectra for linear (a) and circular (b) polarisation. The different colours correspond to different target thicknesses.

Spectral measurements of optical transition radiation (OTR) from the rear of the target also show a defined peak at 527 nm. This demonstrates the 2ω bunching of electrons, indicating that J×B heating is a dominant acceleration mechanism for linear polarisation. In the case of circular polarisation this peak at 2ω decreases in intensity[6].

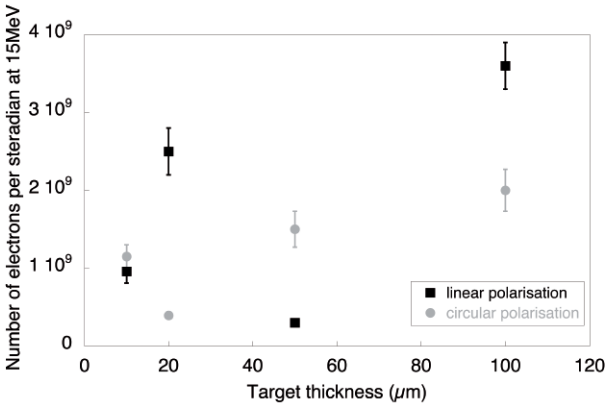

Figure 3. Number of electrons per steradian at 15 MeV energy, plotted against target thickness. The squares indicate linear polarisation and the circles correspond to circularly polarised laser light.

In figure 4 two trends can be observed: 1) larger T_{eff} for linear polarisation 2) increase of T_{eff} with foil thickness. The grey box indicates the target thicknesses that are thicker than half the laser pulse length.

The dependence on laser polarisation has been seen before (by the author) in an experiment with ultrathin (50 and 200 nm) foils. In said experiment, the electron spectra were observed at 40° off laser propagation axis, and showed a decrease of maximum electron energy as well as effective temperature by a factor of two for the case of circular polarisation.

This can be explained by a decrease of the J×B heating for circular polarisation, as the high frequency component of the ponderomotive force (Lorentz force) is turned off. This reduction of J×B heating leads to a decrease in T_{eff} for circular polarisation. In the case of linear polarisation the electrons can be accelerated to above the ponderomotive potential ($p_{max} > a_0 mc$), whereas for the circular polarisation the ponderomotive potential determines the maximum energy that electrons can gain ($p_{max} = a_0 mc$).

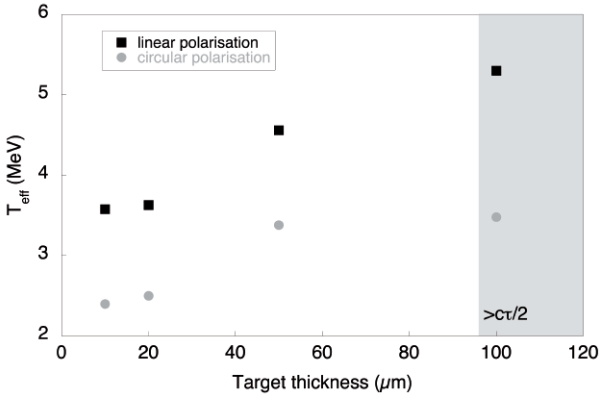

Figure 4. Effective temperatures plotted against target thickness for linear (squares) and circular polarisation (circles). The grey box indicates the thickness threshold above which the target is thicker than half the laser pulse length.

In our case, the circular polarisation is not purely circular, but rather elliptical, since we are hitting the target at a slight angle. This could explain the small difference between linear and 'circular' polarisation.

Independent of the polarisation we observe that the effective temperature increases with target thickness. One might think that this trend is due to an attenuation effect for thicker targets. However, if this were the case, one would expect a decrease in number for all energies of electrons with increasing thickness. The observed increasing number of electrons suggests that it is not merely a range effect (see figure 3).

One possible explanation could be the effect of recirculating electrons on the absorption mechanism. Recirculation of electrons occurs when the electrons are reflected at the target surface by a self-induced sheath field [7]. This affects thin targets stronger than thick targets, since the electron bunch length is approximately the same as the laser pulse length, $c\tau$. For recirculation in thin ($l < c\tau/2$) targets, the effective electron density of hot electrons increases. This is demonstrated by proton acceleration being better for thinner targets. For thick targets, $l > c\tau/2$ (i.e. 100 μm), the electrons overlap only locally at the target edge, therefore no significant increase in electron density appears. The laser ends before the recirculating electrons reach the front surface again [8]. This suggests that returning electrons affect the mechanism of energetic electron generation at the front surface.

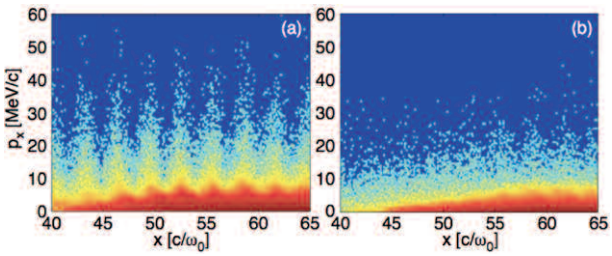

Figure 5. Phase space diagrams, for electrons in the laser direction at 750fs into the interaction. p_x is the momentum in the laser direction (x). Linear polarisation (a) shows bunching at 2ω. This bunching cannot be observed for circular polarisation (b).

Simulations

Simulations are under way to get better insight into the processes going on. The code we are using is the 2D3V particle-in-cell code OSIRIS.

For the first simulations presented here, a stationary box is used to observe the interaction of a laser pulse, a_0=8.7, with an over-dense plasma.

The plasma has a density of 50 n_c and is 5 μm in dimension (30grid cells). The laser beam has a gaussian profile of 0.5 ps duration. The computational grid has longitudinal (x) and transverse (y) dimensions of 21 μm. The target is placed 8.4 μm into the box. The simulations are done with linear as well as circular laser polarisation.

Figure 5 shows the phase space at 750 fs into the simulations for linear (a) and circular (b) polarisations. For the case of linear polarisation (with the electric field in the plane of the simulation) one can observe bunching of the electrons at 2ω in the laser direction, which indicates J×B heating to be the acceleration mechanism. For the case of circular polarisation (figure 5b), the bunching of the electrons disappears, showing very clearly that the J×B heating is turned off. This reflects in the effective temperatures comparable to the experimental data. For circular polarisation we obtain a temperature of 3.4 MeV (for electrons with energies greater than 6 MeV), and for the linear polarised case 5.6 MeV. Though higher than the measured values, the ratio of electron beam temperature between linear and circular polarisations agrees with that obtained experimentally.

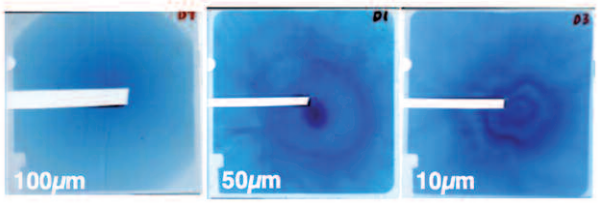

Figure 6. Proton stack data for different target thicknesses.

Proton data

Simultaneous ion measurements, in greater detail discussed in another report in this volume [9], show that the lowest maximum energy is observed for the thickest target (i.e. 100 μm) [8]. For this 'thick' target, we observe a very smooth proton beam profile.

For linear polarisation and thinner targets (10, 20 and 50 μm) the features in the proton data are rings, similar to those seen previousl by Clark *et al.* [1]. These annular rings increase in number as the target thickness decreases. The circular pattern also disappears for higher proton energies and is most visible at low energies. Indeed the number of rings seems to follow the number of transitions of the target made by the relativistic electrons within the duration of the laser pulse. This implies that the generation of the rings is also intrinsically tied to the recirculation of hot electrons within the target.

Conclusions

We have studied the electron acceleration from gold foils ranging from thicknesses of 10 to 100 μm, using different laser polarisations. Two major trends are observed. One trend being the turn off of the J×B heating for the case of circular polarisation, independent of target thickness. The second trend is the thickness dependence of the effective temperature. We observe a decrease of the temperature with decreasing target thickness, for both laser polarisations. This trend appears to be connected to the recirculation of the electrons and its effect on the energy absorption. Simulations are under way to gain better insight into the processes going on in the described interactions.

Acknowledgements

The authors acknowledge the assistance of the Central Laser Facility staff at the Rutherford Appleton Laboratory in carrying out this work. This work was supported by the UK Engineering and Physical Science Research Council (EPSRC). We gratefully acknowledge the OSIRIS consortium which consists of UCLA/IST(Portugal)/USC for the use of OSIRIS.

References

1. E. Clark *et al.*, *Phys. Rev. Lett.* **84**, 670-673 (2000).
2. R. A. Snavely *et al.*, *Phys. Rev. Lett.* **85**, 2945-2948 (2000).
3. S. C. Wilks and W. L. Kruer, *IEEE Journal of Quantum Electronics*, **33**(11) 1954 (1997).
4. F. Brunel, *Phys. Rev. Lett.*, **59**, 52 (1987).
5. S. C. Wilks, *Phys.Fluids B* **5**(7), 2603 (1993).
6. C. Bellei, private communications (2008).
7. A. Mackinnon *et al.*, *Phys. Rev. Lett.* **88**, 215006 (2002).
8. Y. Sentoku *et al.*, *Phys. Plasmas*, **10** (5), 2009 (2003).
9. C. Palmer, RAL Report 2008/09.